Shear thickening in low-concentration solutions of wormlike micelles. I. Direct visualization of transient behavior and phase transitions

Y. T. Hu, Philippe Boltenhagen and D. J. Pine

Citation: Journal of Rheology **42**, 1185 (1998); doi: 10.1122/1.550926
View online: https://doi.org/10.1122/1.550926
View Table of Contents: https://sor.scitation.org/toc/jor/42/5
Published by the The Society of Rheology

Shear thickening in low-concentration solutions of wormlike micelles. I. Direct visualization of transient behavior and phase transitions

Y. T. Hu and Philippe Boltenhagen[a)]

Department of Chemical Engineering, University of California, Santa Barbara, California 93106-5080

D. J. Pine[b)]

Departments of Chemical Engineering and Materials, University of California, Santa Barbara, California 93106-5080

(Received 19 February 1998; final revision received 26 May 1998)

Synopsis

Shear thickening of low-concentration solutions of wormlike micelles is investigated using simultaneous rheological and visualization measurements. Shear-induced structures (SISs) are directly visualized in transparent Couette cells using a laser light scattering technique similar to dark-field microscopy. From these measurements, four different regimes of behavior are identified. In regime I, which occurs below a critical shear stress σ_c, the shear rate increases monotonically with stress and no shear thickening or SISs are observed. In regime II, which occurs for stresses greater than σ_c but less than σ_s, SISs nucleate inhomogeneously and grow from the inner cylinder of the Couette cell. In this regime, the steady state shear rate initially decreases with increasing stress and then increases again as the stress is raised. The steady state in regime II is characterized by two coexisting states separated by a cylindrical interface (concentric with the Couette cylinders). Near the inner cylinder, viscous SISs are observed, while near the outer cylinder, a much less viscous fluid similar to the original micellar solution is observed. The steady state in regime II is observed only under conditions of controlled stress. In regime III, which occurs for stresses above σ_s but below σ_f, SISs nucleate homogeneously throughout the shear cell and appear to fill the gap. Regime IV is characterized by the fracture of SIS and is observed at σ_f. The shear-thickening transition bears many similarities to a phase transition as opposed to a simple hydrodynamic instability. [S0148-6055(98)00405-2]

I. INTRODUCTION

Shear thickening of very low concentration solutions of wormlike micelles has been studied intensely since the early 1980s [Gravsholt (1980); Rehage and Hoffmann (1982); Rehage *et al.* (1986); Kalus *et al.* (1989); Hofmann *et al.* (1991); Hu *et al.* (1993); Hu and Matthys (1995); Liu and Pine (1996), Protzl and Springer (1997)]. In these studies, many key features of the phenomena have been documented, and a picture has emerged in which the shear-thickening is thought to result from the formation of some kind of

[a)]Present address: Laboratoire d'Ultrasons et de Dynamique des Fluides Complexes, URA au CNRS no. 851, Université Louis Pasteur-rue Blaise Pascal, 67070 Strasbourg, France.
[b)]Author to whom all correspondence should be addressed (electronic mail: pine@engineering.ucsb.edu).

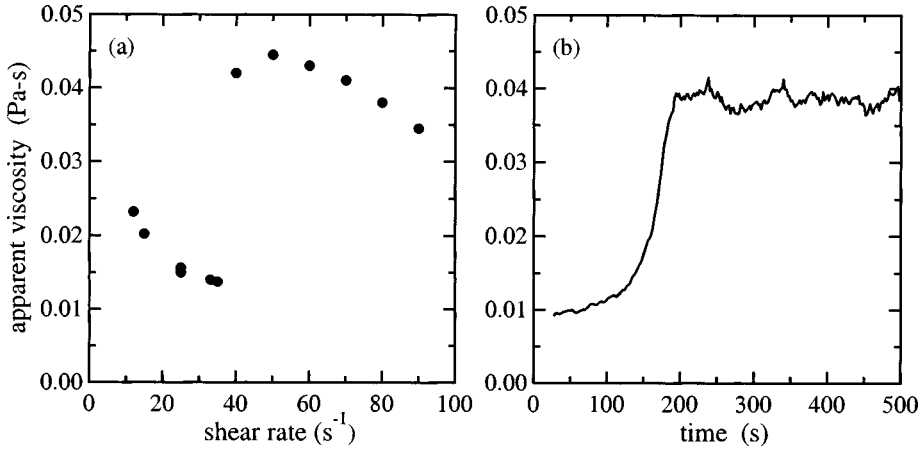

FIG. 1. Typical rheological data illustrating shear thickening in low-concentration wormlike micellar solutions. (a) Steady state viscosity shear rate. Above a critical shear rate, $\dot{\gamma}_c = 37\ \mathrm{s}^{-1}$, the solution exhibits an abrupt increase in the steady state viscosity. (b) Temporal response of a wormlike micellar solution subjected to a constant shear rate $\dot{\gamma} = 80\ \mathrm{s}^{-1}$. The induction time before which little change in the viscosity is observed is $t_1 \cong 60$ s and the plateau time when the viscosity reaches its steady-state value is $t_p \cong 190$ s.

shear-induced structures. In spite of much work, however, the character of these shear-induced structures remains vague and the origin of the shear thickening observed in these systems is not understood.

In this and a companion article (Part II), we report the results of a series of experiments using a new light scattering approach which allows us to directly visualize the formation of shear-induced structures. By performing simultaneous visualization and rheological measurements, we are able to directly correlate known rheological changes in the samples with previously unknown structural changes. In doing so, we identify four distinct regimes, characterized by different rheological behavior and by different kinetics in the formation of the shear-induced structures. These new results provide a kind of ''road map'' to shear thickening which we believe will provide valuable guidance to understanding the microscopic structural origins of shear thickening in very low-concentration wormlike micellar solution.

A. Shear thickening in low-concentration micellar solutions

The basic phenomena of shear thickening in very low-concentration wormlike micellar solutions is summarized in Fig. 1. In Fig. 1(a), we plot a steady state viscosity as a function of shear rate. These data are characteristic of what is typically observed in these systems. At shear rates below some concentration-dependent critical shear rate $\dot{\gamma}_c$, the system exhibits a relatively small viscosity which is comparable to or a few times greater than the solvent (water) viscosity. This indicates that the system can be either just below or just above the overlap concentration (the overlap concentration for these systems is typically just a few mM). The viscosity decreases or is nearly independent of shear rate in this regime, depending on whether the concentration is above or below the overlap concentration. In either case, when the shear rate is increased above the critical shear rate, the apparent viscosity suddenly increases to a value which is 2–50 times greater than that observed below the critical shear rate. As the shear rate is increased further above $\dot{\gamma}_c$, the viscosity may be relatively constant over a range of shear rates but ultimately decreases.

One of the more puzzling features of the shear thickening observed in these micellar systems is that the increase in viscosity observed above $\dot{\gamma}_c$ can take a very long time to develop. This is illustrated in Fig. 1(b), where we show the viscosity as a function of time following the application of a finite shear rate (greater than $\dot{\gamma}_c$) to a well-rested sample. In this case, the viscosity of the system remains relatively constant for a long period of time before beginning to increase. This time of latency, often called the ''induction time'' t_I, can range from seconds to tens of minutes, depending on the concentration, and typically corresponds to the system undergoing a total strain of about $10^3 - 10^4$. Thus, the induction time is approximately inversely proportional to the shear rate [Hu *et al.* (1993); Boltenhagen *et al.* (1997a)]. Once the viscosity begins to rise, it develops slowly and reaches a steady state plateau value after a time t_p which is comparable to t_I. It is also important to note that the induction and plateau times depend on the flow geometry. For example, Hu and Matthys (1995) found that the induction and plateau times decrease when the gap in a Couette flow cell is increased.

The shear-thickened state is characterized by large temporal fluctuations of the viscosity, as shown in Fig. 1(b). This is a universal feature of all the rheological data for shear thickening in these systems. The fluctuations are usually largest near the critical shear rate, but large fluctuations have also been reported far above the onset of shear thickening [Hu and Matthys (1995)].

One of the most surprising features of shear thickening in these systems is the very low concentrations at which these phenomena occur. Shear thickening has been observed in systems with surfactant concentrations as low as 100 ppm by weight (0.01 wt. %). Moreover, the fractional increase in viscosity is largest for the lowest concentrations (note, however, that the system must be above the critical micelle concentration for any effect to be observed). In fact, the shear-thickening effect is not usually observed for surfactant concentrations exceeding a few thousand ppm.

These phenomena—the large increase in viscosity, the long induction and plateau times, the geometry-dependent rheological behavior, the large temporal fluctuations of the viscosity in the shear-thickened state, and the very low concentrations at which shear thickening occurs—are characteristic of a large number of *low-concentration* wormlike micellar solutions. The origin of these phenomena is not understood. This situation is in sharp contrast with that of wormlike micellar solutions at higher concentrations, where the shear-thickening behavior disappears, and where there exists, to varying degrees, an understanding of the rheology based on modified reputation ideas [Cates and Candau (1990)] or based on hydrodynamic instabilities and flow-induced phase transitions [Spenley *et al.* (1993); Makhloufi *et al.* (1995); Britton and Callaghan (1997); Porte *et al.* (1997)].

For low-concentration solutions of wormlike micelles, Rehage and Hoffmann [Rehage and Hoffmann (1982)] have suggested that shear thickening may be a kind of nonequilibrium shear-induced phase transition. It has also been suggested that hydrodynamic instabilities may play an important role in the shear-thickening behavior observed at low concentrations. Recently, there have been some preliminary attempts to develop theories which incorporate ideas about nonequilibrium phase transitions and hydrodynamic instabilities [Olmsted and Lu (1997); Porte *et al.* (1997)]. Based on the data currently available, however, it is difficult to determine whether a description involving a nonequilibrium phase transition or a hydrodynamic instability is more appropriate. One of the purposes of this work is to help clarify this situation by introducing a new experimental probe which can help to distinguish between a shear-induced phase transition and a hydrodynamic instability.

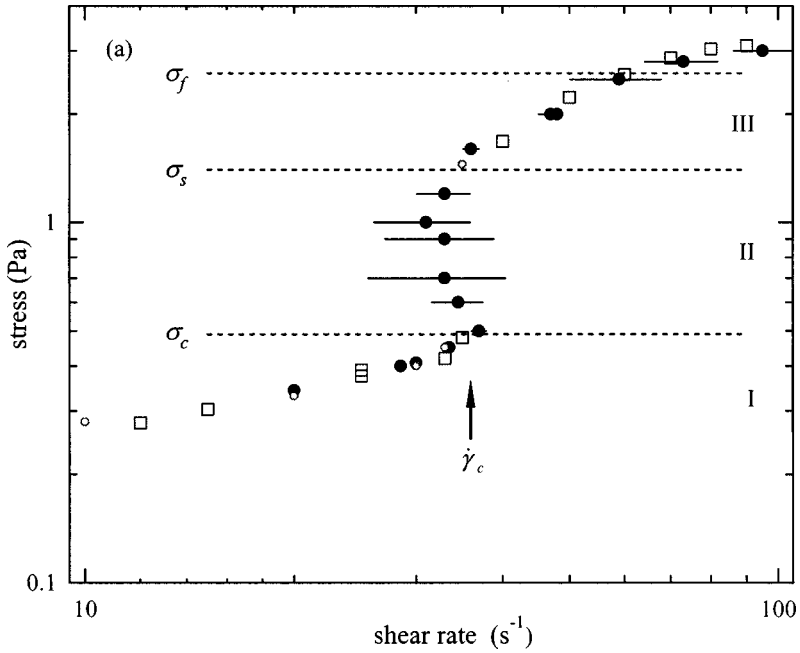

FIG. 2. Summary of the steady state rheology for constant applied stress (solid circles) and shear rate (open squares). The dashed lines indicate the different rheological regimes of behavior. The small open circles locate the final stress/shear-rate pairs for the quenches plotted in Fig. 16.

B. Overview

While the picture we develop of shear thickening in this and a companion paper (Part II) grows out of previous work on low-concentration wormlike micellar solutions, it is sufficiently different from previous descriptions that it is useful to outline our basic results at the outset. As stated earlier, we identify four distinct regimes that are realized by steadily increasing the level of the applied shear *stress*. These four regimes are characterized by different rheological behavior and different *kinetics* in the formation of the shear-induced structures. The four regimes can be distinguished by their steady-state rheology, which is summarized in Fig. 2. Regime I occurs at low shear stresses (below σ_c) and shear rates (below $\dot{\gamma}_c$) and is not much different from the equilibrium fluidlike solution of wormlike micelles apart from the fact that the micelles tend to align with the imposed direction of shear flow. Regime II occurs over an intermediate range of stresses $\sigma_c < \sigma < \sigma_s$ and is observed in steady state only under conditions of controlled shear stress. The steady state in regime II is unique in that the shear rate first *decreases* as the stress is increased above σ_c, and then once again increases as the stress is further increased. Shear-induced structures nucleate inhomogeneously near the inner cylinder of our Couette cells in regime II and can coexist with the fluidlike micellar solution observed in regime I. Regime III occurs above a shear stress σ_s and above the shear rate $\dot{\gamma}_c$. Shear-induced structures are also observed in regime III but they nucleate homogeneously throughout the shear cell. Under conditions of controlled shear rate, the steady state behavior passes directly from regime I to regime III; thus, coexistence of the shear-induced structures and the fluidlike micellar solution is observed only as a transient. Under controlled stress, the lower stress part of regime II may be regarded as a state in which regimes I and III coexist. Our data support the idea that the transition between

regimes I and III can be described as a kind of nonequilibrium phase transition. Finally, regime IV occurs at the highest applied shear stresses and is characterized by a mechanical breakdown of the viscous phase of regime III. This mechanical breakdown corresponds to a fracturing of the bulk viscous phase of regime III and can cause elastically driven hydrodynamic instabilities in the system.

In this article, we are concerned with the transition from regime I to regime III and with the intermediate states of regime II. In particular, we are concerned with the mechanism or mechanisms by which the transition occurs and whether regimes I and III represent fundamentally different phases characterized by different structures or whether they simply represent different ''branches'' of a multi-valued constitutive equation with the same underlying structure. A related issue is whether the shear-thickening transition involves some kind of viscoelastically driven hydrodynamic instability. Various mechanisms and pictures have been suggested in the context of this and related phenomena; in order to guide the development of a theoretical model of shear thickening in these systems, it is important to establish which, if any, of these ideas is supported by the experiment. In the following article (Part II), we will focus on the rheology of regime III and on the mechanical breakdown that occurs at the transition from regime III to regime IV.

II. EXPERIMENT

A. Materials

The surfactant investigated in this study is tris (2-hydroxyethyl) tallowalkyl ammonium acetate (TTAA) [$CH_3(CH_2)_nN(C_2H_4OH)_3Ac$] obtained from AKZO Chemicals (Ethoquad T/13-50). It is a mixture of surfactants with an average molecular weight of 454 g/mole, containing mainly C_{16} and C_{18} alkyl chain surfactants. The master fluid is in liquid form and contains 50% surfactant, 36% isopropanol, and 14% water by weight. The master fluid was dissolved in purified water (produced in house with a Barnstead E-Pure system). Sodium salicylate (NaSal, 2-hydroxyl benzoate, from Aceto, Inc.) was added to produce an equimolar solution of TTAA and NaSal (7.5 /7.5 mM TTAA/NaSal). All materials were used as received. Solutions were stirred with a magnetic stirrer for several hours and kept at room temperature for at least 12 h prior to use.

We chose to use TTAA instead of a better known surfactant such as cetyltrimethylamonium bromide (CTAB) because the equimolar TTAA/NaSal system shows significant shear thickening over a wider range of concentrations and because it has significantly shorter relaxation times, making it much more convenient to use. For example, a shear-thickened solution of CTAB/NaSal can take up to several hours to relax back to its equilibrium state [Liu and Pine (1996)] whereas the longest relaxation time for a 7.5/7.5 mM TTAA/NaSal solution is less than 10 min.

B. Instrumentation

Figure 3 shows a schematic diagram of the experimental setup for simultaneous visualization and rheological measurements. A Rheometrics DSR controlled stress rheometer with a torque range of 10^{-6}–10^{-2} N m was used with a custom made transparent coni-cylinder flow cell. The diameter of the inner and outer cylinders are 23.51 and 25.91 mm, respectively, resulting in a gap of 1.2 mm. The height of the inner cylinder is 55 mm. A water bath (not shown) was built around the flow cell to control temperature. Experiments were performed at 22.5 ± 0.3 °C.

For the visualization experiment, the light source was a Coherent Innova 300 laser operating at a power of about 70 mW. The incident light is focused by a spherical lens and then spread out by a cylindrical lens to produce a thin vertical sheet of light which

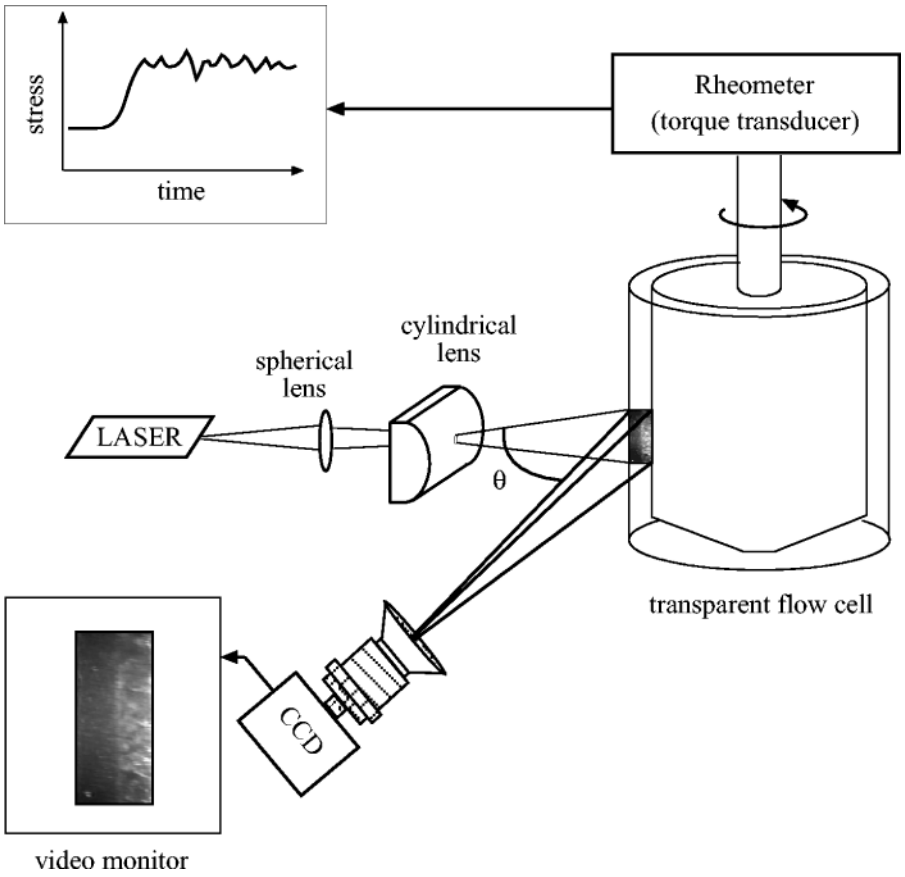

FIG. 3. Schematic of experimental setup used to make simultaneous visualization and rheological measurements. For the visualization measurements, a laser beam is focused by a spherical lens and then expanded with a cylindrical lens to illuminate the sample in the gap of a transparent glass Couette cell. The incident light is approximately perpendicular to the flow direction. Light scattered through approximately 90° is imaged onto a CCD camera and recorded using a VCR. Rheological measurements are made using a controlled stress or controlled shear-rate rheometer.

illuminates a cross section of the sample. The illuminated volume is typically 30 mm high, 0.1 mm thick, and spans the gap of the Couette cell (which is 1.2 mm). The sheet of light is oriented such that a unit vector normal to the sheet points approximately in the flow direction. Light from the sheet is scattered by *fluctuations* in the surfactant concentration [Berne and Pecora (1990)]. That is, larger concentration fluctuations cause an increase in the intensity of scattered light. Light scattered through approximately 90° is imaged onto a charge coupled device (CCD) camera (AVC-D7 by Sony) and recorded on a VCR. A zoom lens (model CM3500 by Raynox) is used to adjust the focus such that an image of light scattered from the sheet is produced on the CCD device. All visualization experiments were carried out simultaneously with rheological measurements in the same flow cell. The rheometer was used both in controlled stress and controlled strain rate modes.

A Rheometrics ARES rheometer was also used for some of the controlled shear rate experiments and for measurements of the frequency dependence of the linear viscoelastic storage and loss moduli $G'(\omega)$ and $G''(\omega)$, as well as the complex viscosity $\eta^*(\omega)$.

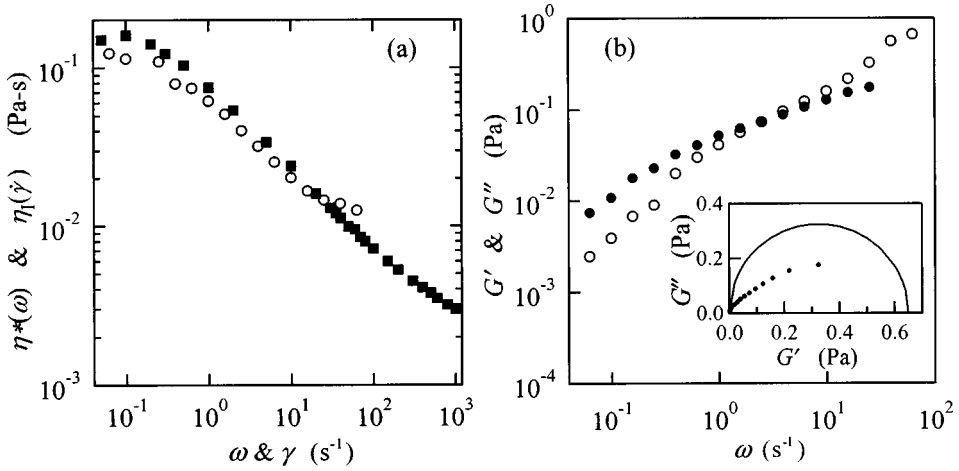

FIG. 4. (a) Induction viscosity $\eta_I(\dot\gamma)$ (solid squares) and dynamic complex viscosity $|\eta^*(\omega)|$ (open circles) as functions of shear rate and frequency, respectively, for a 7.5/7.5 mM TTAA/NaSal solution. The two data sets coincide so that the Cox–Merz rule is obeyed. (b) $G'(\omega)$ (open circles) and $G''(\omega)$ (solid circles) as a function of frequency. Inset: Cole–Cole plot of same data showing non-Maxwellian behavior.

This rheometer has a torque range of $4\times10^{-7}-10^{-2}$ N m. A coni-cylinder geometry was used with inner and outer cylinder diameters of 32.0 and 34.0 mm, respectively. The height of the inner cylinder is 32.3 mm and the cone angle is 0.040 rad.

III. RESULTS

A. Near-equilibrium weak flow behavior

We characterized our samples by first measuring their rheological response near equilibrium. Figure 4(a) shows plots of the complex viscosity $\eta^*(\omega)$ as a function of angular frequency and of the ''induction'' viscosity $\eta_I(\dot\gamma)$ as a function of shear rate for a sample with a concentration of 7.5/7.5 mM TTAA/NaSal. The complex viscosity $\eta^*(\omega)$ was measured in the linear viscoelastic region under small-amplitude oscillatory flow. The ''induction'' viscosity $\eta_I(\dot\gamma)$ was measured under steady shear and was obtained during the period of time prior to the shear-induced increase in the apparent viscosity (see Fig. 1). For shear rates less than the critical shear rate, this ''induction'' viscosity corresponds to the steady state viscosity. These measurements represent near-equilibrium solution properties in the absence of any shear-induced structures. The data superimpose and confirm the validity of the Cox–Merz rule. We note that the zero-shear-rate viscosity is 0.15 Pa s or 150 times larger than the solvent (water) indicating that the micelles are overlapping. The frequency-dependent linear viscoelastic data are replotted in Fig. 4(b) in terms of the moduli $G'(\omega)$ and $G''(\omega)$ with a Cole–Cole plot of the data in the inset. The data do not follow a semicircle indicating that the dynamic moduli do not exhibit simple Maxwell behavior. The dominant relaxation time is a few seconds.

B. Controlled stress flow

For controlled-shear-stress experiments, the shear stress σ is fixed by the application of a constant torque to the inner cylinder of the Couette cell and the shear rate $\dot\gamma$ is measured. If the viscosity of the sample $\eta(t)$ changes as a function of time under flow, the shear rate $\dot\gamma(t)$ changes such that the stress $\sigma = \eta(t)\dot\gamma(t)$ remains constant.

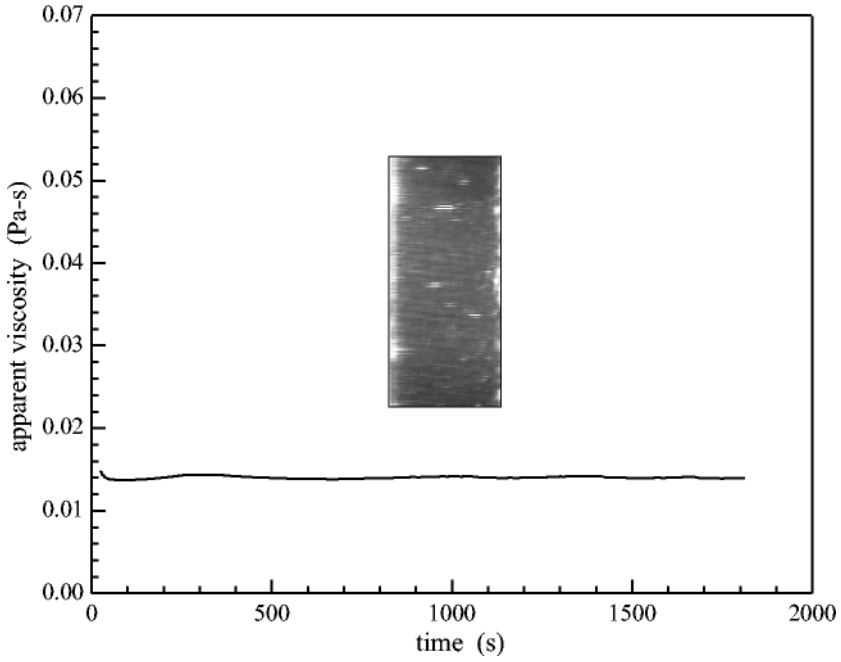

FIG. 5. Time evolution of the apparent viscosity at a stress of 0.4 Pa which is below the critical stress $\sigma_c \approx 0.49$ Pa. There is no shear thickening and no shear-induced structures are observed.

1. Transient behavior

In a transient start-up experiment, we apply a fixed stress to a well-rested solution and monitor the response by simultaneously measuring the time-dependent shear rate and recording an image of the scattered light with a video camera recorder. In general, we present the results of the rheological measurements as an apparent viscosity defined as $\eta(t) \equiv \sigma/\dot{\gamma}(t)$. We emphasize that this is an apparent viscosity (and an apparent shear rate) because, as we shall see, the flow inside the shear cell is not always homogeneous. Great care is taken to assure that data are acquired until a true steady state is achieved. However, the determination of what constitutes a true steady state is complicated by the fact that the steady state is often characterized by large time-dependent fluctuations in the apparent viscosity. Thus, one must wait sufficiently long to be certain that the observed fluctuations are characteristic of the steady state.

Figure 5 shows the temporal evolution of the apparent viscosity along with a light scattering image at steady state for an applied stress of 0.40 Pa. The image was obtained by digitizing a frame taken from a continuous CCD camera recording. Black corresponds to the lowest light scattering intensity and white to the highest. The bright edges and the sporadic bright spots in the gap are caused by scattering from the wall and trace impurities in the sample. In this figure, there is no significant change in the viscosity and the image remains dark throughout the flow, indicating a homogeneous sample in which there are no new structures.

When the shear stress is increased above a certain critical value $\sigma_c \approx 0.49$ Pa, we begin to see changes in both the viscosity and the scattering images, as shown by the data in Fig. 6 obtained for $\sigma = 0.6$ Pa. After an induction time $t_I \approx 150$ s, the measured viscosity begins to increase (note that since the stress is held constant, an *increase* in the measured viscosity corresponds to a *decrease* in the apparent shear rate). A short time

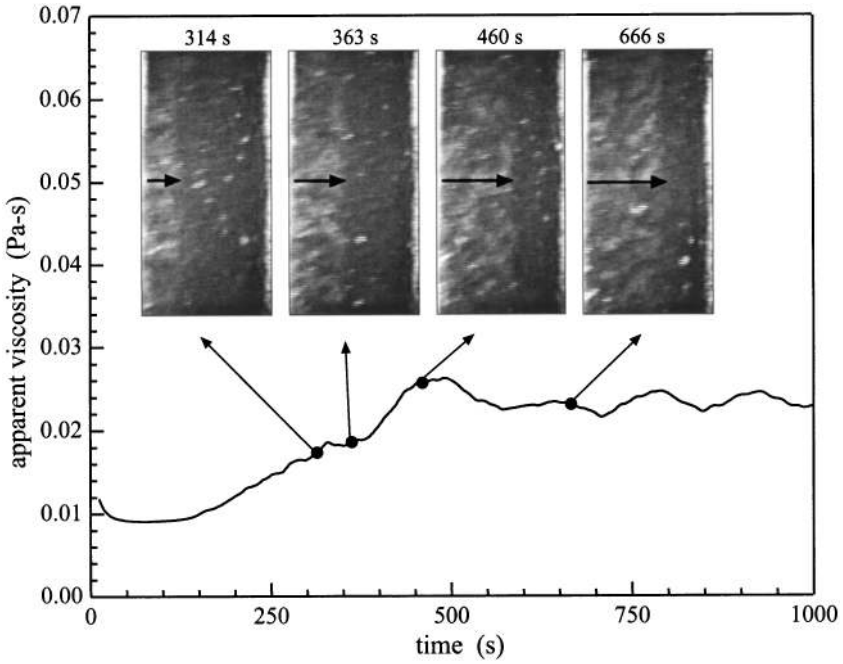

FIG. 6. Time evolution of the apparent viscosity and scattering images after a stress of 0.6 Pa is applied. The inner cylinder of the Couette cell is on the left and the outer cylinder is on the right of each light scattering image (in this and in all subsequent figures). The arrows indicate the position of the front of the shear-induced structure (SIS). The increase in the apparent viscosity is accompanied by an increase in the thickness of the SIS.

later, new shear-induced structures (SISs), different from the original bulk solution, begin to form at the *inner cylinder*, as shown in the first image (obtained at 314 s). The SISs are characterized by an increased scattering intensity with the black arrows in each of the images indicating how far the SIS extends into the gap. The original micellar solution is to the right of the SIS front.

As time increases, the SIS front moves toward the outer cylinder filling an ever expanding fraction of the Couette cell gap. Comparing the four images to the time-dependent apparent viscosity shown in Fig. 6 shows that the temporal increase in the thickness of the SIS corresponds, at least qualitatively, to the temporal increase in the viscosity. After a period of about 10 min, the SIS stops growing and the apparent viscosity reaches a plateau. In the plateau region, the thickness of the SIS exhibits small fluctuations which are synchronous with the fluctuations in the apparent viscosity. The interface between the SIS and the rest of the solution fluctuates about a constant position which indicates that a steady state is achieved in which there is coexistence between the SIS and the original micellar solution. The nucleation and growth of the SIS is reminiscent of a first order phase transition which occurs by *inhomogeneous* nucleation of the new phase at the inner cylinder of the Couette cell.

When the transient stress experiment is repeated at higher stresses, up to approximately 1.4 Pa, essentially the same process described above repeats itself. That is, the SIS first appears at the inner cylinder of the Couette cell and grows towards the outer cylinder. In addition, the SIS appears and grows more quickly as the stress in increased. This behavior is illustrated in Fig. 7 where we plot the position of the SIS front as a function of time after the application of a constant shear stress and observe that the thickness of the SIS advances linearly with time. For the higher applied stresses, the growth curve

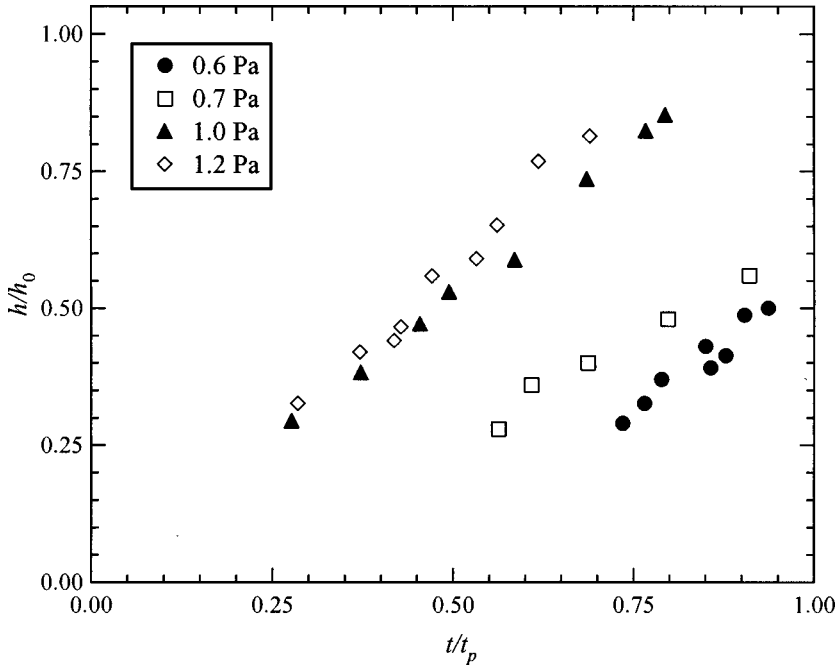

FIG. 7. Advance of the front of the SIS across the gap of the Couette cell under controlled stress (all stresses in regime II). The advance of the front for different stresses is always linear to within experimental uncertainty. At the higher stresses, the growth curves extrapolate backwards through zero time suggesting that nucleation of the SIS occurs essentially immediately after the application of shear stress. At lower stresses, the growth curves extrapolate to a finite time suggesting a period of latency prior to nucleation of the SIS.

extrapolates backwards through the origin, suggesting that the nucleation and growth commences immediately upon the inception of shear flow. By contrast, for the lowest stress (just above σ_c) the curve extrapolates backwards in time to a finite value, suggesting there is a true period of latency before the SIS begins to grow.

For applied stresses at or below approximately 1.0 Pa, the SIS ultimately stops short of the outer cylinder and a steady state is achieved in which the SIS coexists with the original micellar solution. For an applied stress of 1.2 Pa, the SIS still originates at the inner cylinder and grows outward, but the SIS ultimately appears to fill the entire gap of the Couette cell, as shown in Fig. 8. Again, the temporal progression of the SIS across the gap corresponds qualitatively to the temporal increase in the apparent viscosity. The steady state behavior of the solution is discussed further in Sec. III B 2.

When the stress applied in a transient start-up experiment is increased above a second critical stress $\sigma_s \approx 1.4$ Pa, the mechanism for SIS formation changes. The SIS no longer nucleates *inhomogeneously* near the inner cylinder, but instead nucleates *homogeneously* throughout the gap of the Couette device. This is illustrated in Fig. 9 which shows data taken for $\sigma = 1.6$ Pa. In this case, the SIS first appears at approximately 31 s and is visible throughout the entire gap even though the viscosity has just begun to increase. A mere 3 s later, at 34 s, the light scattering from the SIS has become much brighter and the SIS clearly fills the gap. Nevertheless, the viscosity is still not much higher than the initial level. This suggests that the individual domains of SIS formed at this stage are isolated from each other; that is, the SISs do not percolate across the gap. This interpretation is consistent with the fact that the intensity of the scattered light is greatest around the time $t = 34$ s, when the new phase is first nucleated throughout the sample. During

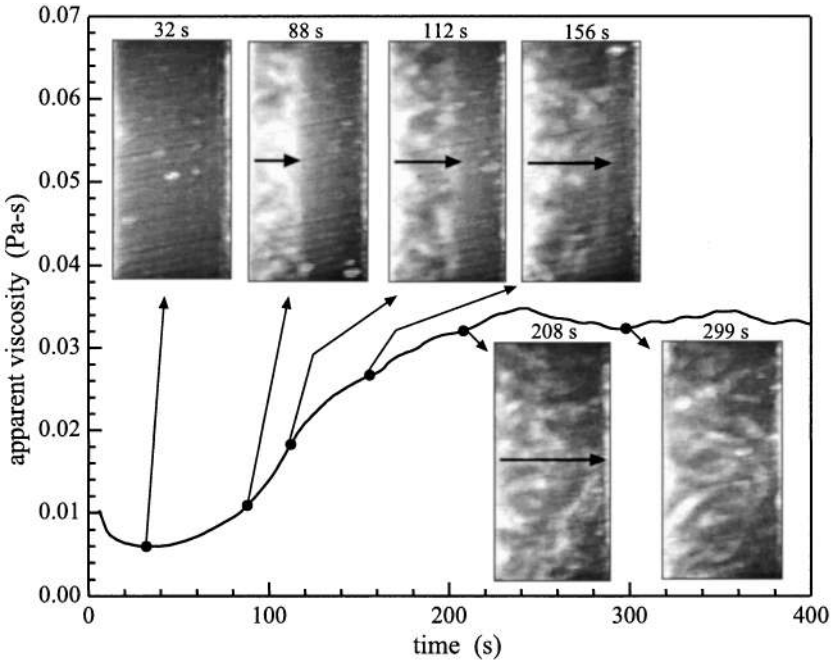

FIG. 8. Time evolution of the apparent viscosity and scattering images after a stress of 1.2 Pa is applied. The arrows indicate the position of the front of the shear-induced structure (SIS). The front advances farther and more quickly than it does for a lesser stress of 0.6 Pa (see Fig. 6).

this time period, the nucleating domains of SIS are isolated from each other and produce large density fluctuations giving rise to an increased scattered light intensity (see Sec. II B). After 50 s, the SIS light scattering image is dimmer indicating that the SIS has become more homogeneous than at 34 s. In the intervening time, the viscosity has become much larger than it was initially. The more homogeneous scattering and the large viscosity suggests that the SIS domains are largely interconnected at this stage. After 86 s, the scattering image becomes even more homogeneous while the viscosity reaches a plateau. The formation of the SIS is complete at this stage. In this final stage, the light scattering image is brighter than it was for the fluidlike phase, but somewhat dimmer than it was when the SIS first nucleated throughout the gap. This process of SIS formation (when $\sigma > \sigma_s$) is reminiscent of a first order phase transition which occurs by *homogeneous* nucleation of the new phase. This is to be contrasted with the behavior we observed when $\sigma_c < \sigma < \sigma_s$ in which the transition to the new phase occurs by *inhomogeneous* nucleation of the SIS at the inner cylinder of the Couette cell. It should be noted, however, that for stresses just below σ_s it is difficult to distinguish between homogeneous and heterogeneous nucleation. In this case, the SISs appear to form homogeneously, or very nearly homogeneously, throughout the gap and then to contract very rapidly, by as much as 30%, toward the inner cylinder, after which the scattered light intensity increases as the SIS interface grows toward the outer cylinder.

2. Steady state behavior

Figure 10 summarizes the steady state behavior of the apparent viscosity for data obtained under constant applied shear stress. The same protocol was followed for each data point, as described above. The steady state rheological behavior, summarized in Fig.

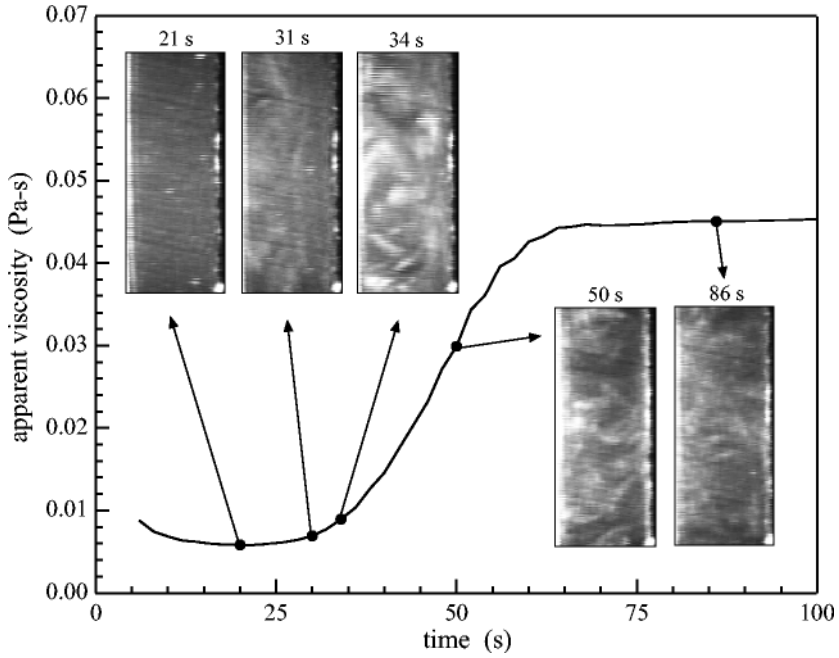

FIG. 9. Time evolution of the apparent viscosity and light scattering images after a stress of 1.6 Pa is applied. Note that the SIS appears homogeneously throughout the gap at about 31 s just as the apparent viscosity begins to increase. The SIS is clearly visible throughout the gap at 34 s, when the apparent viscosity is still well below its ultimate steady state value.

10, can be divided into four regimes corresponding to the same four regimes discussed earlier in the context of the transient behavior. In regime I, below $\sigma_c \approx 0.49$ Pa, the stress decreases with shear rate. In this regime, the stress and viscosity remain low and no SIS is formed. In regime II, $\sigma_c < \sigma < \sigma_s \approx 1.4$ Pa, the steady state apparent viscosity increases continuously as the stress is increased. In regime III, $\sigma_s < \sigma < \sigma_f \approx 2.6$ Pa, the steady state apparent viscosity saturates and becomes independent of the applied shear stress to within experimental uncertainty (the uncertainty is the result of intrinsic fluctuations in the steady state shear rate and not instrumental limitations). In regime IV, $\sigma > \sigma_f$, the apparent viscosity decreases sharply with increasing stress.

The light scattering images reveal additional information about the structure of the steady state behavior in the four regimes. In regime I, the solution is homogeneous. In regime II, the behavior is more complex. When the shear stress is below 0.9 Pa, a sharp planar interface is formed between the SIS and the fluid phase (more precisely, the interface forms a cylinder concentric with the cylinders of the Couette cell). The position of this interface fluctuates in time about a well-defined average value. The magnitude of the fluctuations is small for stresses just above σ_c, as illustrated in Fig. 6 for a shear stress of 0.6 Pa. As stress is increased, the steady state mean position of the interface moves towards the outer cylinder and the magnitude of the fluctuations about its mean position increases. The apparent viscosity exhibits a corresponding increase in its mean value and in the magnitude of the fluctuations about this mean. The fluctuations in the interfacial position are largest for a stress of 0.9 Pa, as illustrated in Fig. 11. In this case, the fluctuations are fairly periodic with a period of about 10 min, whereas at lower shear stresses, the period of the fluctuations is more random (see Fig. 6). In both cases, the fluctuations in the thickness of the SIS and in the apparent viscosity track each other. The

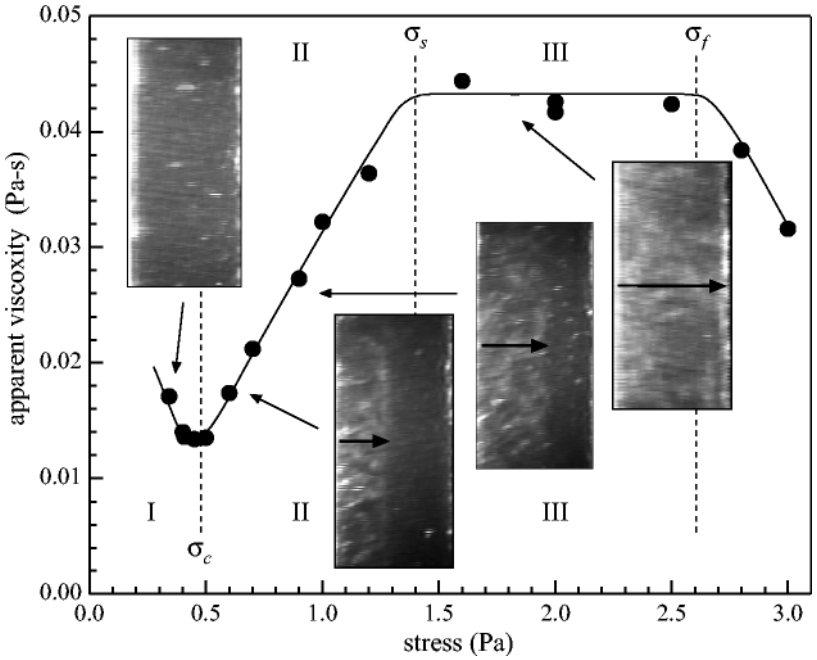

FIG. 10. Steady state apparent viscosity vs stress for data obtained under controlled shear stress. The light scattering images show the absence of SIS in regime I, the coexistence of the SIS with the fluid phase in regime II, and a gap filled with SIS in regime III. The arrows indicate the extent of the SIS.

origin of these fluctuations, however, is not understood. When the shear stress is increased to 1.1 Pa, the SIS appear to fill the gap. The mean value of the steady state mean viscosity continues to increase with increasing stress, however, and fluctuations in the apparent viscosity continue to be evident throughout regime II. This suggests that the SISs are either unconsolidated near the outer cylinder or that they are easily broken apart by the applied shear stress.

When the stress is increased into regime III, where the steady state apparent viscosity saturates, the SIS fills the gap. We note that the level of stress σ_s, at which the viscosity saturates, appears to be the same stress that separates the regime of ''heterogeneous nucleation'' of SIS from the regime of ''homogeneous nucleation.'' Thus, there is a direct correlation between the different steady states and the two different nucleation mechanisms.

C. Controlled shear rate flow

For controlled shear rate experiments, the shear rate $\dot{\gamma}$ is fixed and the shear stress σ is measured. Once again, we present the data in terms of an apparent viscosity, $\eta(t) = \sigma(t)/\dot{\gamma}$. If the viscosity of the sample $\eta(t)$ changes under flow, the stress changes in time such that the shear rate $\dot{\gamma} = \sigma(t)/\eta(t)$ remains constant.

1. Transient behavior

When the shear rate is below a critical value of $\dot{\gamma}_c$ [$\approx 37\ s^{-1}$, Fig. 1(a)], there is no significant shear thickening. When the shear rate is increased above $\dot{\gamma}_c$, the sample begins to shear thicken and the SIS begins to form at the inner cylinder and grows outwards towards the outer cylinder, as shown in Fig. 12 ($\dot{\gamma} = 80\ s^{-1}$). The growth of

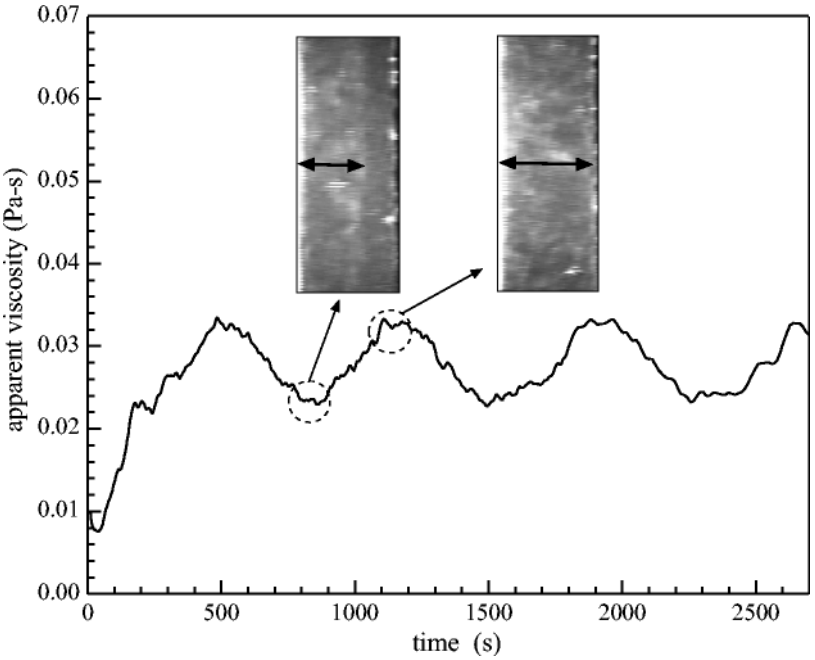

FIG. 11. Time evolution of the apparent viscosity and scattering images after a stress of 0.9 Pa is applied. At this stress, there are large slow fluctuations in the apparent viscosity and in the thickness of the SIS in the gap. The period is about 10 min. The maximum change in the steady state SIS thickness is about 34%. The magnitude of the viscosity fluctuations is about 35%, and is almost identical with the magnitude of the SIS fluctuation.

the SIS is similar to that observed under controlled stress flow in regime II, that is, when $\sigma_c < \sigma < \sigma_s$. Once again, the apparent viscosity and the thickness of the SIS grow synchronously with each other until the late stage of SIS formation, when the correspondence between the two breaks down. At 175 s, for example, the SIS appears to have filled the gap, whereas the viscosity has not yet reached the plateau. We found that the higher the shear rate, the larger the discrepancy between the time the SIS fills the gap and the time when the viscosity reaches its plateau.

This behavior can be understood in terms of the heterogeneous and homogeneous nucleation phenomena discussed above. When a constant shear rate is initially applied to a well-rested equilibrium sample, it develops a stress which is consistent with the viscosity of the equilibrium solution. If the shear rate is slightly greater than $\dot{\gamma}_c$ (e.g., $\dot{\gamma} \approx 1.05\dot{\gamma}_c$), the initial stress will be slightly greater than σ_c but less than σ_s. This will induce inhomogeneous nucleation of the SIS at the inner cylinder. Since the SIS has a greater viscosity than the original solution and since the *shear rate* is held constant, the stress will increase. This increase in stress causes the SIS to grow even thicker, which in turn further increases the stress. This process continues, resulting in a kind of *positive feedback* that causes the SIS to grow even thicker; this further increases the stress in the solution [Boltenhagen *et al.* (1997b); Porte *et al.* (1997)]. At some point, the SIS grows to be thick enough such that the stress exceeds the stress σ_s required for homogeneous nucleation. At that point, the SIS appears to fill the remainder of the gap very rapidly as a result of the homogeneous nucleation which occurs when $\sigma > \sigma_s$, However, the stress (or apparent viscosity) has not yet reached its steady state level because the homogeneously nucleated SIS has not percolated across the remainder of the gap. As the

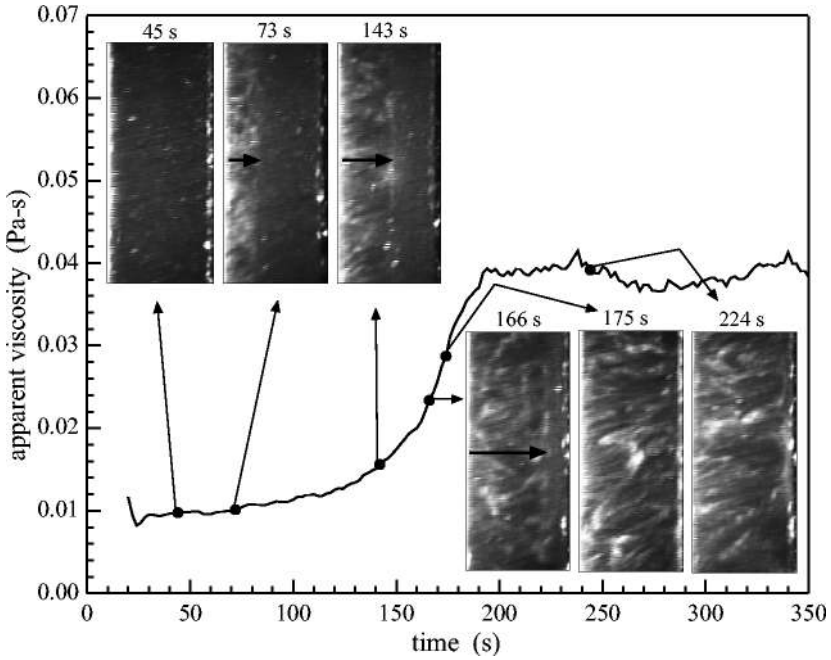

FIG. 12. Transient apparent viscosity and scattering images under a constant applied shear rate of 80 s^{-1}. Arrows in the scattering images indicate the positions of the SIS front. The apparent viscosity and thickness of the SIS appear to grow approximately together. Note that the SIS appears to fill the gap, however, at about 166 s, or about 20 s before the apparent viscosity reaches its steady state value.

homogeneously nucleated SIS percolates, the stress continues to rise until the steady state level of stress is attained and the gap is completely filled with the fully developed SIS.

The effect of this feedback mechanism can be seen in the growth of the SIS front with time. In contrast to the linear rate of growth observed under controlled stress (see Fig. 11), the rate of growth of the SIS front increases with time, as illustrated in Fig. 13 by the upward curvature of the data obtained under controlled shear rate. The increasing rate of growth of the SIS front reflects the increase in stress as the gap fills with the SIS.

We also observe a very interesting phenomenon below, but very near the critical shear rate $\dot{\gamma}_c$. In this region, the apparent viscosity increases slowly with time and eventually stops at a plateau. The magnitude of this increase, however, is very small compared to the large increase that occurs above $\dot{\gamma}_c$. This behavior is illustrated in Fig. 14 where we show traces of the time-dependent apparent viscosity obtained for shear rates of 20, 25, and 35 s^{-1}. The traces obtained at the two lower shear rates show no remarkable increase in the apparent viscosity with time. By contrast, the data obtained at a shear rate of 35 s^{-1} increases slowly with time and then levels off. The increase is small, and in fact, no permanent new structures are observed in the gap of the Couette cell, except that occasionally traces of structures appear at the inner cylinder surface for a short time and then disappear. This phenomena appears to be very sensitive to the initial surface condition of the flow cell. It is most noticeable when the flow cell has been cleaned and then used without allowing the solution to remain in the cell for a long time. These observations suggest that the small increase in stress may represent some kind of pre-transitional ''wetting'' of the inner surface by an incipient SIS.

It is striking that when inhomogeneous nucleation occurs, i.e., when $\sigma_c < \sigma < \sigma_s$, the SIS always appear to nucleate at or near the inner cylinder. An obvious

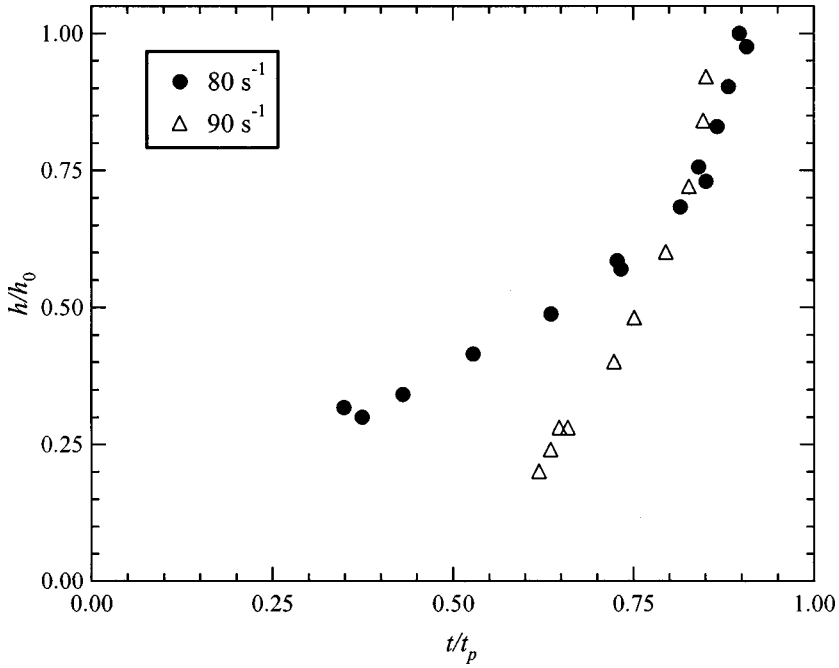

FIG. 13. Advance of the front of the SIS across the gap of the Couette cell under constant shear rate. Note the acceleration in the advance of the front with time, consistent with an increase in stress as the SIS advances across the gap under constant shear rate.

explanation for this observation is that the stress is greatest at the inner cylinder. Since the $\sigma \propto r^{-2}$, the stress is approximately 20% greater at the inner than at the outer cylinder. If this is indeed the reason that the SIS appears to nucleate at the inner cylinder, then it is not obvious that what we observe is heterogeneous nucleation in the usual sense. Normally, heterogeneous nucleation is associated with a process in which the presence of impurities or boundaries promote nucleation by locally lowering the nucleation barrier at nucleation sites. In our case, it may simply be that the stress is higher at the inner cylinder. While we cannot rule out this possibility, our observation that the surface condition of the inner cylinder seems to affect whether or not we observe the ''wetting'' behavior described above which seems to favor a picture of heterogeneous nucleation in the usual sense. Nevertheless, the SISs are first observed at the inner cylinder whenever $\sigma_c < \sigma < \sigma_s$, irrespective of whether or not any pre-transitional behavior is observed and the issue of just what type of nucleation process is occurring here is open to interpretation.

Since the stress in the Couette cell decreases as a function of radius, one might ask if the stable steady state interface between the SIS and the fluid phase which is observed under constant stress is simply a manifestation of a lower subcritical shear stress at larger radii. This is not the case, however, as can readily be determined from our measurements. For example, in Fig. 6 we show the development of a stable SIS phase which extends approximately 2/3 across the gap of the shear cell for an applied stress of 0.6 Pa at the inner cylinder. Since $\sigma \propto r^{-2}$, the stress at the outer cylinder is 0.5 Pa which is significantly greater than the critical stress $\sigma_c = 0.4$ Pa. Thus, the sample does not separate into two parts because the stress is subcritical in the outer part. Instead, it seems that the role of the mild stress gradient in these experiments is similar to the role of gravity in a

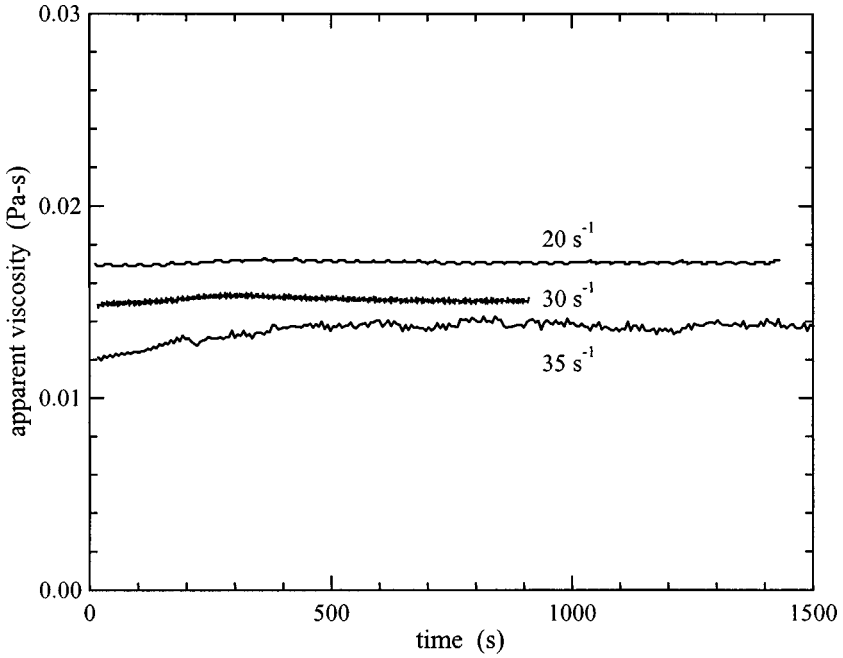

FIG. 14. Transient apparent viscosity and scattering images under a constant applied shear rate for shear rates below the critical shear rate ($\dot{\gamma}_c = 37\ s^{-1}$). Note the small, slow increase in the apparent viscosity just below the critical shear rate (i.e., for $\dot{\gamma} = 35\ s^{-1}$).

binary liquid mixture which is cooled into the two phase region of the phase diagram. Just as gravity serves to separate the two phases of a binary liquid mixture, which are in thermodynamic equilibrium according to their relative densities, the mild stress gradient in our experiments serves to separate the two phases of the surfactant solution according to their relative elasticity (i.e., the more elastic SISs are drawn to the inner cylinder [Larson (1992)].

2. Steady state behavior

In Fig. 15, we show the steady state rheological behavior and two representative SIS images for the system as a function of the shear rate. Below the critical shear rate $\dot{\gamma}_c$ ($\approx 37\ s^{-1}$), the viscosity remains low and no stable SIS is observed. Above $\dot{\gamma}_c$, the viscosity jumps to a much higher level and SIS fills the gap. Thus, in contrast to the continuous evolution of the steady state behavior under controlled stress, the system adopts one of two steady states under controlled shear rate: a system void of SIS or filled with SIS. The mechanism by which this occurs can be understood in terms of the positive feedback mechanism discussed Sec. III C 1.

D. Comparison of steady state behavior under controlled stress and controlled shear rate

The difference in the steady state behavior between controlled shear rate and controlled shear stress is most evident when we plot stress versus apparent shear rate for both kinds of experiments, as shown in Fig. 2. Once again, three distinct regimes can be identified. In regime I, which is below the critical stress σ_c for controlled stress and below the critical shear rate $\dot{\gamma}_c$ for controlled rate, the two data sets superimpose. The

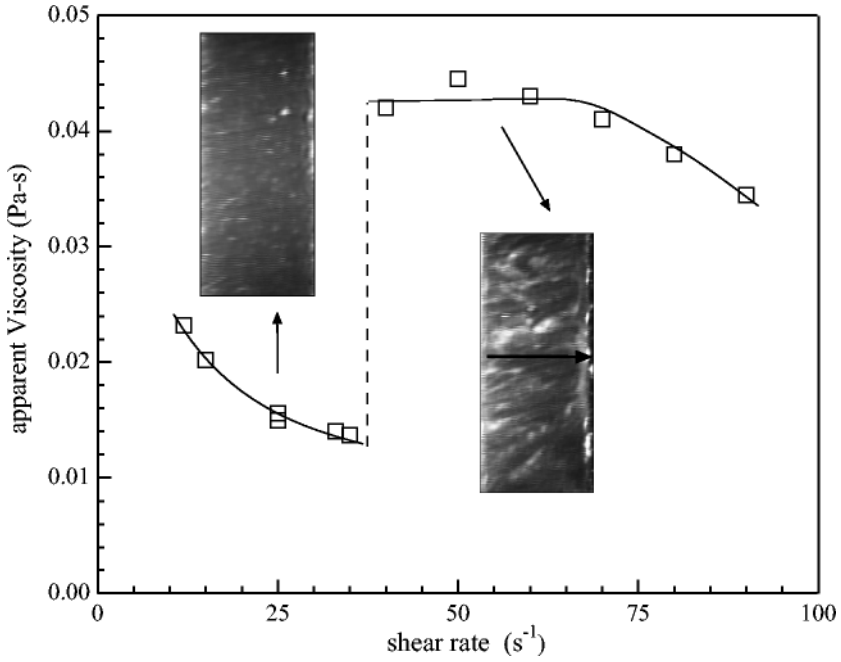

FIG. 15. Steady state apparent viscosity vs shear rate for data obtained under controlled shear rate. The scattering images show that for shear rates less than the critical shear rate, there are no SISs in the gap. Above the critical shear rate, the SISs always fill the gap.

critical stress appears to be identical to the stress corresponding to the critical shear rate. This region represents the behavior of the equilibrium micellar solution where no SIS is formed. Note that near the critical shear rate, the curve shows a slight upward trend. This corresponds to the small increase of viscosity near the critical shear rate, as shown in Fig. 14 which was attributed to pre-transitional wetting behavior.

Regime II corresponds to the region between σ_c and σ_s. In this regime, new micellar structures formed under controlled stress grow progressively as the stress increases. The controlled stress curve is continuous and exhibits a re-entrant behavior. By contrast, the controlled shear rate curve bypasses regime II and exhibits a discontinuous jump from regime I to regime III ($\sigma > \sigma_s$). Thus, regime II is not observed in *steady state* constant shear rate measurements.

In region III, the two steady state data sets for constant stress and constant shear rate once again superimpose.

E. Shear-rate quench experiments

In this section, we explore the behavior of the system when the shear rate is suddenly decreased, starting from a shear rate above $\dot{\gamma}_c$ (i.e., regime III). Prior to quenching, the system is sheared several minutes at a shear rate of 60 s^{-1} until the steady state is achieved; the steady state stress is approximately 2.5 Pa ($> \sigma_s = 1.4$ Pa). The shear rate is then decreased suddenly to some lower shear rate and the temporal evolution of the shear stress is monitored. In Fig. 16 we show the results of several different quench experiments. When the shear rate is decreased from 60 to 35 s^{-1}, the stress falls very rapidly (due to the reduction in shear rate) to about 1.8 Pa and then relaxes to a steady state level of about 1.5 Pa in about 200 s. The stress remains at this relatively high level,

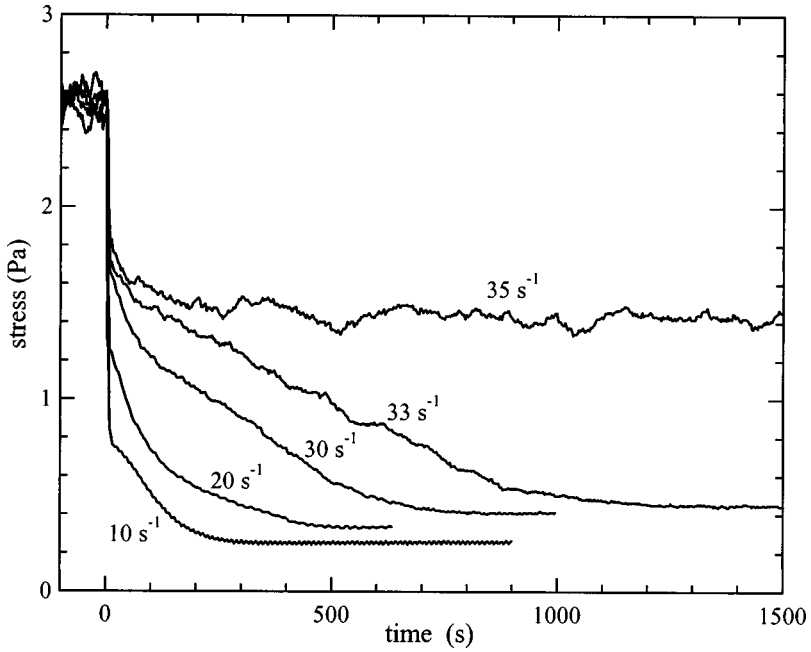

FIG. 16. Time evolution of stress after the shear rate is quenched from 60 s^{-1} to various lower shear rates as indicated in the figure. The coordinates of the final stress/shear-rate pairs are indicated by the small open circles in Fig. 2.

which is greater than σ_s, and does not show any further decrease for as long as the shear is maintained. Thus, the system remains in regime III.

When the shear rate is decreased from 60 to 33 s^{-1}, which is less than $\dot{\gamma}_c$, a rapid decrease in stress (once again, due to the reduction in shear rate) is followed by a much slower decay of the stress to a steady state value of approximately 0.45 Pa, which is below σ_c (= 0.49 Pa). In this case, however, the stress takes approximately 1000 s to relax to its steady state value. When the shear rate is quenched further below $\dot{\gamma}_c$, the stress relaxes faster, as shown in Fig. 16. Thus, for quenches in which $\dot{\gamma} < \dot{\gamma}_c$, we find that the system becomes more metastable and takes longer to reach steady state when the quench shear rate $\dot{\gamma}$ is moved closer to $\dot{\gamma}_c$.

Visualization results for the quench experiments, presented in Fig. 17, provide more insight into the way in which the stress and SIS decay. Immediately following the quench to 33 s^{-1} ($< \dot{\gamma}_c$) there appears to be very little change in the scattering pattern for several hundred seconds. Nevertheless, the stress decreases slowly during this period of time. Even after 369 s, the light scattering image shows that the SIS still appears to fill the gap. Eventually, however, dark areas do emerge and the SIS is observed to retreat across the gap. This retreat begins at the outer cylinder, as shown in the image obtained at 438 s. The stress at which two distinct regions can first clearly be seen is about 1.1 Pa, the same stress at which the SIS first appears to fill the gap in the steady state experiments. As the stress decreases further, the SIS becomes thinner and thinner. These visualization results indicate that two processes occur within the SIS during the quench: first the bulk dissolution of the SIS, and second, the dissolution of the SIS at the interface between the SIS and the solution.

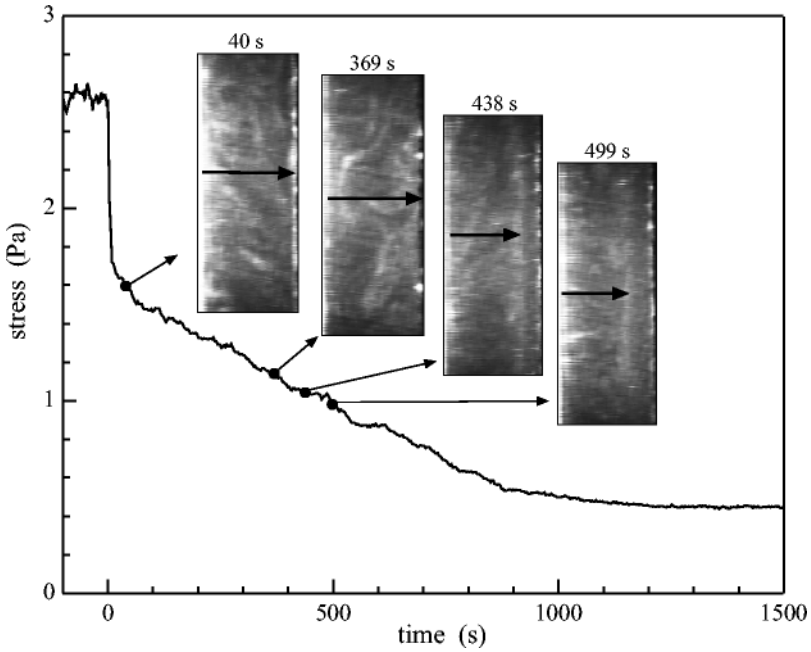

FIG. 17. Light scattering images and time evolution of stress after the shear rate is quenched from 60 to 33 s^{-1}. Note that SIS pulls away from the outer cylinder of the Couette cell (right side of images) at approximately 438 s or when the stress falls below about 1.1 Pa. Arrows indicate the extent of the SIS.

IV. DISCUSSION

Our experiments clearly show that shear thickening in low-concentration surfactant solutions of TTAA/NaSal is characterized by the formation of inhomogeneous structures. We have also performed less extensive experiments on several similar shear-thickening systems, including CTAB/NaSal [Liu and Pine (1996)], and have observed similar behavior. Thus, our results seem to be generic, that is, characteristic of a number of surfactant systems which form long wormlike micelles at low concentrations.

A. Phase transition or mechanical instability

Recently, there has been a great deal of theoretical work on shear-induced phase transitions and inhomogeneous flows in complex fluids [Cates *et al.* (1993); Olmsted and Lu (1997); Porte *et al.* (1997)]. While it is clear from our experiments that these surfactant solutions exhibit inhomogeneous flows and structure formation, it is less clear whether the changes we observe can or should be regarded as a kind of shear-induced phase transition or merely as a mechanical instability. A mechanical instability can result in shear banding (i.e., an inhomogeneous flow field), for example, when the constitutive relation for stress versus shear rate is multi-valued for a given value of stress or strain rate [Cates *et al.* (1993)]. A shear-induced phase transition is also expected to be associated with a multi-valued constitutive relation. However, a phase transition is generally also associated with a microscopic structural transition in which some fundamental symmetry of the system changes. While there is strong evidence that the low-viscosity ''phase'' of these sheared surfactant solutions consists of shear-aligned wormlike micelles, the microstructure of the viscous SIS is less well understood. Nevertheless, there are several experimental observations which, in our opinion, suggest that shear thickening in these systems may be the result of an underlying shear-induced phase transition.

One of the strongest results favoring a description of shear thickening based on a shear-induced phase transition is the existence of two distinct mechanisms for the nucleation of the SIS. For constant stress flows, the SIS nucleates inhomogeneously, starting at the inner cylinder of the Couette cell and growing outwards, when $\sigma_c < \sigma < \sigma_s$ (regime II). When $\sigma > \sigma_s$ (regime III), the SIS nucleates homogeneously throughout the gap of the Couette cell. This behavior is very reminiscent of a first order phase transition, such as the liquid–gas transition in simple liquids.

It is also worth noting that these same nucleation criteria are valid for controlled shear rate flows. That is, when the applied shear rate is sufficiently large to produce a stress greater than σ_s (regime II), the SIS nucleates at the inner cylinder and grow outwards. When the stress exceeds σ_s, the growth of new SIS switches to homogeneous nucleation. Thus, the occurrence of the transition does not seem to be controlled by the dynamical path, but simply by achieving well-defined levels of shear stress, σ_c and σ_s. Thus, σ_c and σ_s appear to be state variables.

This viewpoint is further supported by the quench experiments, in which the shear rate is suddenly decreased from a shear rate greater than $\dot{\gamma}_c$ to a shear rate less than $\dot{\gamma}_c$. In this case, the SIS appear to dissolve homogeneously as long as the instantaneous stress exceeds σ_s. The dissolution mechanism switches over to an inhomogeneous dissolution mechanism soon after the instantaneous stress falls below σ_s. Furthermore, when the shear rate is quenched to a value very near, but just below $\dot{\gamma}_c$, the dissolution process proceeds very slowly indicating that the driving force back to the SIS-free steady state is very weak. Thus, the dissolution of the SIS seems to be more consistent with the dissolution of a high-stress phase rather than a hydrodynamic instability.

In a similar fashion, the development the SIS occurs very slowly when the shear stress exceeds the critical shear stress σ_c by a small amount. For these cases, the time for the SIS to develop is several hundred seconds, which is much longer than any rheological time scale (a few seconds) for the micellar solution. Thus, in both increasing or decreasing the shear stress through σ_c, the response time is much longer than any rheological time scale.

One particularly intriguing observation is the small, slow increase in the apparent viscosity that we observed when a shear rate just below but very near $\dot{\gamma}_c$ is applied to the well-rested equilibrium solution. We interpreted this as a pre-transitional ''wetting'' layer which forms on the inner surface of the Couette cell. This is very similar to pre-transitional wetting behavior observed in binary liquid mixtures and polymer solutions near a phase boundary. This interpretation seems to be supported by our observation that this behavior can be suppressed by not using an adequate cleaning procedure for the cells walls.

A related phenomenon which seems to support a phase-transition mechanism is the coexistence of the two stable ''phases'' under conditions of controlled stress when $\sigma_c < \sigma < \sigma_s$ (regime II). A particularly compelling observation is the fact that the steady state thickness of the SIS seems to be completely determined by the applied level of stress, and not on its dynamical history. Thus, there seems to be an underlying mechanism which divides the system into two parts with a single well-defined interface dividing them. Moreover, there is no evidence that the flow within the two ''phases'' is anything other than simple shear flow. Thus, the SIS seems to represent a new state, whose appearance is controlled by the level of applied stress.

The idea that the SIS represents a new state is further supported by the vastly different rheological properties of the SIS from the original solution. From some preliminary measurements of the velocity profile in regime II, we estimate that the SIS is at least a

factor of 10 more viscous than the fluid phase (see the following article (Part II)). This difference lends support to the idea that the SIS represents a new phase.

The sum total of these data, taken together, make a compelling case for describing shear thickening as a nonequilibrium shear-induced phase transition. Nevertheless, in the final analysis, this idea is only useful insofar as it is an aid in developing a theory which can accurately describe shear thickening in these systems. Perhaps the key unresolved issue for developing a theory is the unknown nature of the microscopic structure of the SIS. Is it some kind of micellar structure essentially similar to the equilibrium micellar solution, or does shear flow cause some kind of fundamental structural change? The rheological measurements we report in the following article (Part II) shed some light on this question and suggest that the SIS possesses a new kind of microstructure. Nevertheless, more experiments are needed to answer this question definitively.

B. Correspondence between the SIS formation and the shear thickening

The data presented in this study, and in particular the light scattering microscopy measurements shown in Figs. 5, 7, and 11, clearly show that there is a close correspondence between the increase in the apparent viscosity and the formation of SIS in the surfactant solution. However, the correspondence is not always simple. For experiments in which the shear rate or stress is suddenly increased, there are essentially three scenarios: (1) In regime II under controlled stress, the growth in apparent viscosity matches the growth in the thickness of the SIS fairly closely. (2) In regime III under controlled stress, this correspondence breaks down almost completely. Instead, the temporal increase in viscosity seems to correspond to the density or homogeneity of SIS. (3) For controlled shear rate, the correspondence between the apparent viscosity and thickness of SIS is valid as long as the stress is lower than σ_s. Once the stress exceeds σ_s, the SIS begin to form throughout the gap. Shortly after this occurs, the sharp boundary between the SIS and the rest of the solution blurs and the SIS very rapidly fills the gap (Fig. 12). At this point, the correlation between the growth in the apparent viscosity and the thickness of the SIS breaks down. This explains why there is a discrepancy in the time between when the SIS appear to fill the gap and when the stress reaches the plateau.

V. CONCLUSION

A significant result of this study is the observation that shear thickening in low-concentration wormlike micellar systems occurs through the inhomogeneous nucleation of viscous structures at moderate stresses and through the homogeneous nucleation at high values of stress. The experiments also reveal that it is the *shear stress* rather than the *shear rate* which controls the steady state in these systems. This allows one to categorize different regimes according to the kinetics of shear thickening and according to the structures that form. In regime I, a relatively low-viscosity phase which exhibits shear thinning is observed, consistent with shear alignment of the micelles. In regime II, a viscous phase is observed to co-exist with the less viscous phase of regime I. The viscous phase is generated by shear and nucleates inhomogeneously from the inner wall in regime II. Regime II is observed under steady state conditions only when the externally applied stress is held constant; coexistence is observed only under transient conditions when the shear rate is held constant. In regime III, the viscous phase nucleates homogeneously and fills the entire volume of the flow cell.

Our results reveal that shear thickening is associated with the growth of shear-induced structures in a manner that shares many similarities with phase transitions observed in equilibrium systems, as discussed in Sec. IV A. Indeed, theories based on analogies with

equilibrium phase transitions are beginning to be developed to describe shear-induced rheological and structural changes in complex fluids [Grand *et al.* (1997); Olmsted and Lu (1997), Porte *et al.* (1997)]. While these theories do not apply directly to the low-concentration surfactant systems that are the subject of this study, our results suggest that such approaches may prove useful in providing a better understanding of shear thickening in micellar solutions.

In this article we have used a light scattering imaging technique with simultaneous rheological measurements to probe shear thickening in very low concentration solutions of wormlike micellar solutions. The primary value of the light scattering technique is that it allows one to directly image the shear-induced structures. This is important because shear thickening in these systems proceeds in a complex fashion. For example, it would be very difficult to ascertain that shear thickening occurs through either inhomogeneous or homogeneous nucleation, depending on the level of shear stress, without some kind of direct visualization technique. An important feature of this technique, which should not be overlooked, is its simplicity. The only requirements are a moderate-power laser (or other light source which can be suitably focused to form a well-defined sheet of light), a transparent shear cell, and a CCD camera.

ACKNOWLEDGMENTS

The authors thank Peter Olmsted, Eric Matthys, and Rachid Makhloufi for useful discussions and Jennifer Politsch for a critical reading of the manuscript. This work was supported by the National Science Foundation under Award Nos. DMR96-32716 (MRL program) and NSF DMR96-25856 (Instrumentation for Materials Research Program).

References

Berne, B. J. and R. Pecora, *Dynamic Light Scattering: With Applications to Chemistry, Biology, and Physics* (Wiley, New York, 1990).

Boltenhagen, P., Y. T. Hu, E. F. Matthys, and D. J. Pine, ''Inhomogeneous structure formation and shear-thickening in worm-like micellar solutions,'' Europhys. Lett. **38**, 389–394 (1997a).

Boltenhagen, P., Y. T. Hu, E. F. Matthys, and D. J. Pine, ''Observation of bulk phase separation and coexistence in a sheared micellar solution,'' Phys. Rev. Lett. **79**, 2359–2362 (1997b).

Britton, M. M. and P. T. Callaghan, ''Two-phase shear band structures at uniform stress,'' Phys. Rev. Lett. **30**, 4930–4933 (1997).

Cates, M. E. and S. J. Candau, ''Statics and dynamics of worm-like surfactant micelles.,'' J. Phys.: Condens. Matter **2**, 6969–6992 (1990).

Cates, M. E., T. C. B. McLeish, and G. Marrucci, ''The rheology of entangled polymers at very high shear rates,'' Europhys. Lett. **21**, 451–456 (1993).

Grand, C., J. Arrault, and M. E. Cates, ''Slow transients and metastability in wormlike micelle rheology,'' J. Phys. II **7**, 1071–1086 (1997).

Gravsholt, S., ''Rheological properties on highly dilute viscoelastic aqueous detergent solutions,'' Proceedings International Congress on Rheology, 1980, Vol. 8, pp. 629–633.

Hofmann, S., A. Rauscher, and H. Hoffmann, ''Shear induced micellar structures,'' Ber. Bunsenges. Phys. Chem. **95**, 153–164 (1991).

Hu, Y. T. and E. F. Matthys, ''Characterization of micellar structure dynamics for a drag-reducing surfactant solution under shear: Normal stress studies and flow geometry effects,'' Rheol. Acta **34**, 450–460 (1995).

Hu, Y. T., S. Q. Wang, and A. M. Jamieson, ''Rheological and flow birefringence studies of a shear-thickening complex fluid—A surfactant model system,'' J. Rheol. **37**, 531–546 (1993).

Kalus, J., H. Hoffmann, S.-H. Chen, and P. Lindner, ''Correlations in micellar solutions under shear: A small-angle neutron scattering study of the chain surfactant *N*-Hexadecyloctyldimethylammonium bromide,'' J. Phys. Chem. **93**, 4267–4282 (1989).

Larson, R. G., ''Flow-induced mixing, demixing, and phase transitions in polymeric fluids,'' Rheol. Acta **31**, 497–520 (1992).

Liu, C.-H. and D. J. Pine, ''Shear-induced gelation and fracture in micellar solutions,'' Phys. Rev. Lett. **77**, 2121–2124 (1996).

Makhloufi, R., J. P. Decruppe, A. Ait-Ali, and R. Cressely, ''Rheo-optical study of worm-like micelles undergoing a shear banding flow,'' Europhys. Lett. **32**, 253–258 (1995).

Olmsted, P. D. and C.-Y. D. Lu, ''Coexistence and phase separation in sheared complex fluids,'' Phys. Rev. E **56**, R55–R58 (1997).

Porte, G., J.-F. Berret, and J. L. Harden, ''Inhomogeneous flows of complex fluids: Mechanical instability versus non-equilibrium phase transition,'' J. Phys. II **7**, 459–472 (1997).

Protzl, B. and J. Springer, ''Light scattering experiments on shear induced structures of micellar solutions,'' J. Colloid Interface Sci. **190**, 327–333 (1997).

Rehage, H. and H. Hoffmann, ''Shear induced phase transitions in highly dilute aqueous detergent solutions,'' Rheol. Acta **21**, 561–563 (1982).

Rehage, H., I. Wunderlich, and H. Hoffmann, ''Shear induced phase transitions in dilute aqueous surfactant solutions,'' Prog. Colloid Polym. Sci. **72**, 51–59 (1986).

Spenley, N. A., M. E. Cates, and T. C. B. McLeish, ''Nonlinear rheology of wormlike micelles,'' Phys. Rev. Lett. **71**, 939–42 (1993).